






Article

Development of Eco-Friendly Mortars Produced with Kaolin Processing Waste: Durability Behavior Viewpoint

Alisson Mendes Rodrigues ^{1,*}, Fabiana Pereira da Costa ², Suellen Lisboa Dias Beltrão ²,
Jucielle Veras Fernandes ², Romualdo Rodrigues Menezes ¹ and Gelmires de Araújo Neves ¹

¹ Laboratory of Materials Technology (LTM), Department of Materials Engineering, Federal University of Campina Grande, Bodocongó, Campina Grande 58429-900, Brazil; romualdo.menezes@ufcg.edu.br (R.R.M.); gelmires.neves@ufcg.edu.br (G.d.A.N.)

² Graduate Program in Materials Science and Engineering (PPG-CEMat), Department of Materials Engineering, Federal University of Campina Grande, Bodocongó, Campina Grande 58429-900, Brazil; fabiana.costa@estudante.ufcg.edu.br (F.P.d.C.); slisboabeltrao@gmail.com (S.L.D.B.); jucielle_fernandes@hotmail.com (J.V.F.)

* Correspondence: alisson.mendes@professor.ufcg.edu.br

Abstract: This study presents the development of new eco-friendly mortar compositions containing kaolin residues (KR) and assesses their durability behavior. Firstly, the natural and calcinated kaolin residues (600 °C, 650 °C, 700 °C, 750 °C, and 800 °C) were characterized by X-ray diffraction (XRD), differential thermal analysis (DTA), granulometric analysis, and surface area. The kaolin residue calcinated at 800 °C was chosen to be added to new compositions of mortar because it presented the best pozzolanic performance. The aging tests accomplished in internal (E_i) and external (E_e) environments were applied in mortars with a mass proportion of 1:2:6 (cement + KR: lime: sand), in which the KR, calcinated at 800 °C, replaced the cement in the mass fraction of 0%, 5%, 10%, 15%, 20%, and 30%. The E_i was performed for 30, 60, 90, 180, and 360 days, and the E_e for 90; 210; 360; and 512 days. After the aging tests were completed, the mortar compositions containing KR were evaluated to determine their mineralogical phases (XRD), compressive strength (CS), and thermal behavior (DTA and thermogravimetry). In summary, the KR addition to the mortar compositions decreases the mechanical resistance to compression; however, mortars with a substitution of 10% and 20% presented resistance values within the minimum limit of 2.4 MPa established by ASTM C 270.

Keywords: kaolin; solid residues; pozzolanic activity; cement mortar; carbonation



Citation: Rodrigues, A.M.; Costa, F.P.d.; Beltrão, S.L.D.; Fernandes, J.V.; Menezes, R.R.; Neves, G.d.A. Development of Eco-Friendly Mortars Produced with Kaolin Processing Waste: Durability Behavior Viewpoint. *Sustainability* **2021**, *13*, 11395. <https://doi.org/10.3390/su132011395>

Academic Editor: Jorge de Brito

Received: 9 August 2021

Accepted: 9 October 2021

Published: 15 October 2021

Publisher's Note: MDPI stays neutral with regard to jurisdictional claims in published maps and institutional affiliations.



Copyright: © 2021 by the authors. Licensee MDPI, Basel, Switzerland. This article is an open access article distributed under the terms and conditions of the Creative Commons Attribution (CC BY) license (<https://creativecommons.org/licenses/by/4.0/>).

1. Introduction

Sustainable construction materials are being increasingly studied to minimize the environmental impacts generated by the civil construction sector. Many studies have targeted alternative materials to replace the use of cement in concretes and mortars to improve their sustainability. This is because the Portland cement production process releases one of the highest CO₂ emission rates in the world. It is estimated that about one ton of carbon dioxide is created for each ton of Portland cement produced [1–3].

Several studies have been carried out using alternative cementitious materials to replace Portland cement in concretes and mortars to mitigate their environmental impacts and reduce costs. Among the alternative materials are fly ash [4–6], blast furnace slag [7–9], eggshell powder [2,10], silica fume [11–13], limestone [14,15], calcium carbide residue [16], and calcined kaolin residue, which is undoubtedly one of the most well known alternative cementitious materials [17]. The kaolinite clay is the main constituent in the kaolin residues. When such residues are submitted to thermal treatment, under controlled conditions, kaolinite dehydroxylation is guaranteed, whereby it transforms itself into an amorphous structure called metakaolinite. Metakaolin can be used in civil construction and added to mortars to act as a material pozzolanic. The main property of a pozzolana is

its ability to react and combine with calcium hydroxide, forming stable compounds with an agglomerating power, such as hydrated calcium silicates and aluminates [17–19].

The positive effects exerted by pozzolans on the mechanical properties and durability of mortars and concretes have been emphasized in several studies. Al-Akhras [20] investigated the sulfate resistance of concretes produced from the mixture of metakaolinite (MK) with Portland cement (PC), at the substitution levels of 5, 10, and 15 wt%, and concluded that such a substitution was beneficial for the resistance to the sulfate, which increases with the increase in MK content in the mixture. Guneyisi et al. [21] used MK to substitute Portland cement at levels of 10 and 20 wt% to improve the performance of the concrete. The authors evaluated the durability properties of samples produced from water absorption (WA), drying shrinkage (DS), and porosity (P) measures, and reported that the incorporation of MK reduced the drying shrinkage deformation and improved the pore structures of the samples. In addition, they observed a decreasing trend in WA with an increase in the MK content.

It is worth mentioning that durability evaluation is undoubtedly the most critical aspect of cementitious material development because, for it to be reliable, knowledge of its conditions of use and its useful life is essential [22–24]. Although the calcined kaolin residue has been extensively studied as a pozzolanic material, studies that addressed the long-term durability behavior of mortars containing kaolin residue are still scarce. Therefore, this work aims to use calcined kaolin residue as a partial substitute for cement in different percentages (0%, 5%, 10%, 15%, 20%, and 30%) in the composition of mortar for coating, and to assess the overall impact on the long-term durability behavior. Mortar durability will be evaluated by natural aging tests in the internal (30, 60, 90, 180, and 360 days) and external (90, 210, 360, and 512 days) environments.

2. Materials and Methods

2.1. Raw Materials

The Portland cement type CPII-F 32 (PC) was used as a binder following the ASTM C150 standard (CIMPOR BRASIL) [25]. This cement was used because it does not have the addition of pozzolan. The other materials used were hydrated lime (HL) (Carbomil); sand (S), with a density of 2.6 g/cm³ and an average particle diameter of 4.8 mm; and kaolin residue (KR) supplied by Caulim Caiçara S/A (Brazil). The as-received kaolin residue was pulverized in a MultiNo[®] (270 M/S/M) compressed air mill for 30 min, and heat-treated for 2 h at different temperatures (600 °C, 650 °C, 700 °C, 750 °C, and 800 °C). The heat treatments were carried out in an electric oven (Flyever Equipment, FE 50 RP) at a heating rate of 5 °C/min⁻¹.

2.2. Preparation and Curing of the Mortar Samples

Samples with a mass proportion of 1:2:6 (cement + KR: lime: sand) were prepared with and without the kaolin residue. In the samples with kaolin residue, the cement was replaced. The mass fractions of Portland cement substitutions by calcined kaolin residue were 0%, 5%, 10%, 15%, 20%, and 30%.

The raw materials were mixed in a mechanical planetary motion mixer for 5 min. After that, water was added to the mixture until the consistency index was 260 ± 10 mm (ASTM C 1437) [26]. The test specimens were molded in a cylindrical mold with the dimensions of 50 mm × 100 mm (diameter × height). After 24 h, the samples were demolded and immersed in water with lime (2% concentration) for 30 days. This procedure was carried out to avoid carbonation. Table 1 provides details of the proportions used for the mortars and the nominal composition of replaced cement.

2.3. Mortar Durability Assessment

Aging tests in internal (E_i) (laboratory) and external (E_e) environments were carried out to evaluate the durability of the two mortar compositions studied. All experiments were carried out in triplicate. The aging test specimens in an internal environment were

kept in a place protected from external climatic actions (a laboratory environment with temperatures between 21 °C and 30 °C, and an air humidity of ~78%) for 30, 60, 90, 180, and 360 days. The test specimens submitted to the aging test in an external environment were kept in a place that permitted their exposure to the environment's natural climatic conditions. The samples from this test were kept in this environment for 90, 210, 360, and 512 days.

Table 1. Nominal composition and percentages of cement replaced by calcined kaolin residue.

Designation	Percentage of PC Replaced by KR (%)	
	PC	KR
M0	100	-
M5	95	5
M10	90	10
M15	85	15
M20	80	20
M30	70	30

2.4. Characterizations

The chemical composition was defined using X-ray fluorescence (Shimadzu, EDX 720). The mineralogical phase characterization was performed by X-ray diffraction (XRD) using a Shimadzu XRD6000 equipment with Cu K α radiation (40kV/30mA), and a goniometer speed of 2 °C/min⁻¹, step of 0.02°, and the JCPDS database. Thermogravimetric (TGA) and differential thermal (DTA) analyses were performed using a BP Engenharia equipment (model RB-300) with a nitrogen atmosphere and heating rate equal to 12.5 °C/min⁻¹. All thermal analyses were performed in platinum crucibles and the temperature range was kept between 25–1000 °C. Before the mineralogical (XRD) and thermal (TGA and DTA) tests, the mortar samples were packed in polyethylene bags to prevent carbonation and the tests were carried out on the same day.

The particle size distribution of kaolin residue was determined by laser diffraction (Cilas, 1064 LD), and the specific area was evaluated using the BET methodology (ASAP 2420 V2.02). The pozzolanic activity (I_{PA}) was measured from test specimens (50 mm x 100 mm) manufactured from two mortar compositions. The first composition, called reference mortar (mortar ref.), only contained Portland cement. In the second composition (mortar KR), 20% of the cement was replaced by calcined kaolin residue. In both compositions, the H₂O/PC or H₂O/(PC + KR) ratio was equal to 0.485, as specified in ASTM C311M [27]. Compressive strength (CS) measurements were performed using test specimens cured for 7, 14, and 28 days, and the I_{PA} value was calculated with the aid of Equation (1):

$$I_{PA}(\%) = \frac{CSM_{KR}}{CSM_{Ref}} \times 100 \quad (1)$$

where CSM_{Ref} (MPa) and CSM_{KR} (MPa) correspond to the CS values measured using the mortar ref. and mortar KR samples, respectively.

After each exposure period (durability tests), compressive strength tests were carried out in accordance with ASTM C39/C39M [28]. All experiments were performed on a universal mechanical testing machine (SHIMADZU, AG-IS) with a loading speed of 0.25 ± 0.05 MPa/s. Mineralogical (XRD) and thermal (TGA and DTA) tests were also carried out to monitor the phase transformations.

3. Results and Discussions

3.1. Raw Materials Characterizations

The chemical compositions of Portland cement type CPII-F 32, hydrated lime, and kaolin residue are listed in Table 2. Figure 1a,b show XRD patterns of Portland cement type CPII-F 32 and of hydrated lime. The mineralogical phases: tricalcium silicate (C3S—3CaO·SiO₂,

JCPDS 49-0442); dicalcium silicate ($C_2S=2CaO \cdot SiO_2$, JCPDS 33-0302); tricalcium aluminate ($C_3A=3CaO \cdot Al_2O_3$, JCPDS 38-1429); iron tetracalcium aluminate ($C_4AF=4CaO \cdot Al_2O_3 \cdot Fe_2O_3$, JCPDS 30-0226); calcium carbonate ($CaCO_3$, JCPDS 05-0586); and calcium sulfate hemihydrate ($CaSO_4 \cdot 1/2H_2O$, JCPDS 0041-0244), were detected in the Portland cement (Figure 1a). In the hydrated lime (Figure 1b) the phases of portlandite ($Ca(OH)_2$, JCPDS 72-0156) and calcite ($CaCO_3$, JCPDS 05-0586) were detected.

Table 2. The chemical composition of Portland cement type CII-F 32, hydrated lime, and kaolin residue.

Raw Materials	Oxides								
	SiO ₂	Al ₂ O ₃	Fe ₂ O ₃	K ₂ O	MgO	CaO	SO ₃	Others	LOI ¹
PC	19.6	10.3	1.1	-	11.5	38.0	8.3	1.5	9.7
HL	1.6	0.6	0.1	0.3	1.6	72.3	-	0.4	23.1
KR	58.8	36.0	0.2	1.6	2.2	-	-	0.4	0.8

¹ LOI—Loss on ignition measured after drying at 110 °C and firing at 1000 °C.

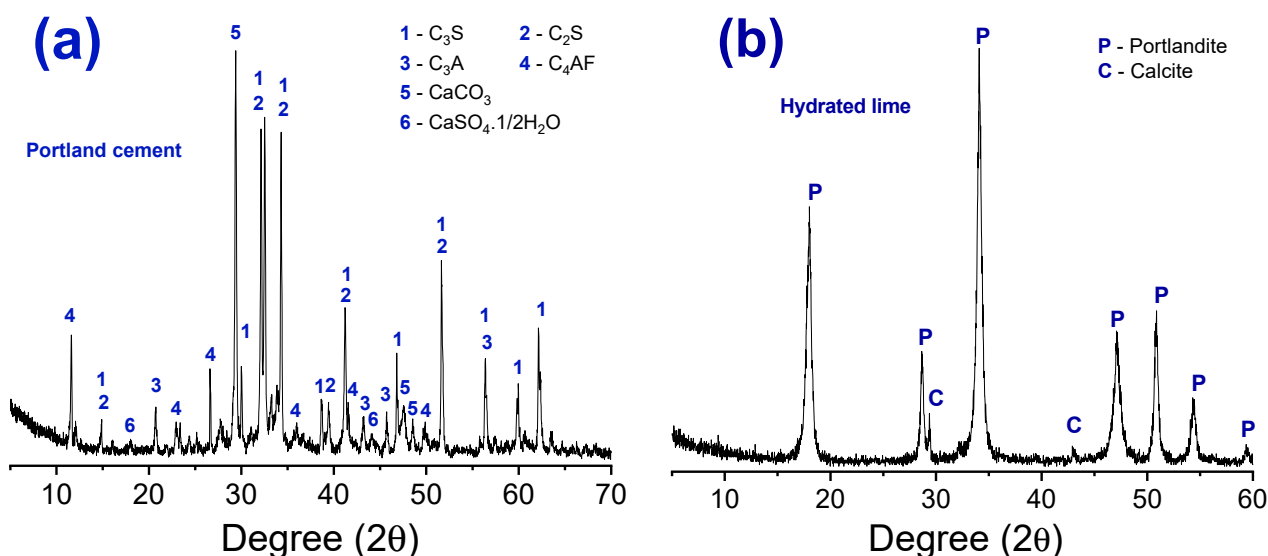


Figure 1. The XRD patterns measured from Portland cement type CII-F 32 (a) and hydrated lime (b).

Figure 2a–f show the XRD patterns of natural and calcined kaolin residues at different temperatures (600 °C, 650 °C, 700 °C, 750 °C, and 800 °C). The mineralogical phases: quartz (SiO_2 , JCPDS 46-1045); mica ($KMg_3(Si_3Al)O_{10}(OH)_2$, JCPDS 83-1808); and kaolinite ($Al_2Si_2O_5(OH)_4$, JCPDS 14-0164) were detected in the natural kaolin residue. Except for kaolinite, all other mineralogical phases were also identified in the calcined kaolin residues. At temperatures above 500 °C, the kaolinite suffers dehydroxylation with the consequent breakdown of the structure, which then forms the metakaolinite ($Al_2Si_2O_5(OH)_4 \rightarrow Al_2O_3 \cdot 2SiO_2 + 2H_2O$). However, the characteristic amorphous band of metakaolin is not evident in Figure 2b–f, due to the relatively high intensity of the quartz peak ($2\theta = 26.64^\circ$).

The DTA curves measured from natural and calcined kaolin residues are shown in Figure 3. The natural kaolin residue has an endothermic peak at around 600 °C, which is characteristic of kaolinite dehydroxylation, giving rise to amorphous metakaolinite [29]. Such a kaolinite dehydroxylation peak (at 600 °C) was not observed in the DTA curves measured from the calcined kaolinite residues. An exothermic peak at 900 °C is related to mullite nucleation [30,31], which was identified in all DTA curves.

The granulometric and surface area analysis of Portland cement particles, hydrated lime, and natural and calcined kaolin residues are listed in Table 3. In general, the natural and calcined kaolin residues presented an average particle diameter between 12.1 µm and 19.0 µm. The specific surface area is a relevant factor in the pozzolanic reaction

since it depends strongly on the structure of the surface and its specific area [32,33]. It is worth remembering that the larger the specific area, the greater the reactivity of the material. Furthermore, the material's specific area tends to be larger if the particle size is smaller [34,35]. A greater fineness of the kaolin residue leads to an improvement in its pozzolanicity. Therefore, the calcined kaolin residue at the temperature of 800 °C was used to prepare the mortar compositions investigated in this study because it had the smallest average particle diameter (12.8 μm) and the largest specific area (25.95 m^2/g). Huang et al. [29] evaluated the influence of the calcination temperature (500–1000 °C) on the pozzolanic activity in the kaolin residues from southwest China. They found that the best calcination temperature for converting the kaolin residue into metakaolin with a high pozzolanic index was 800 °C.

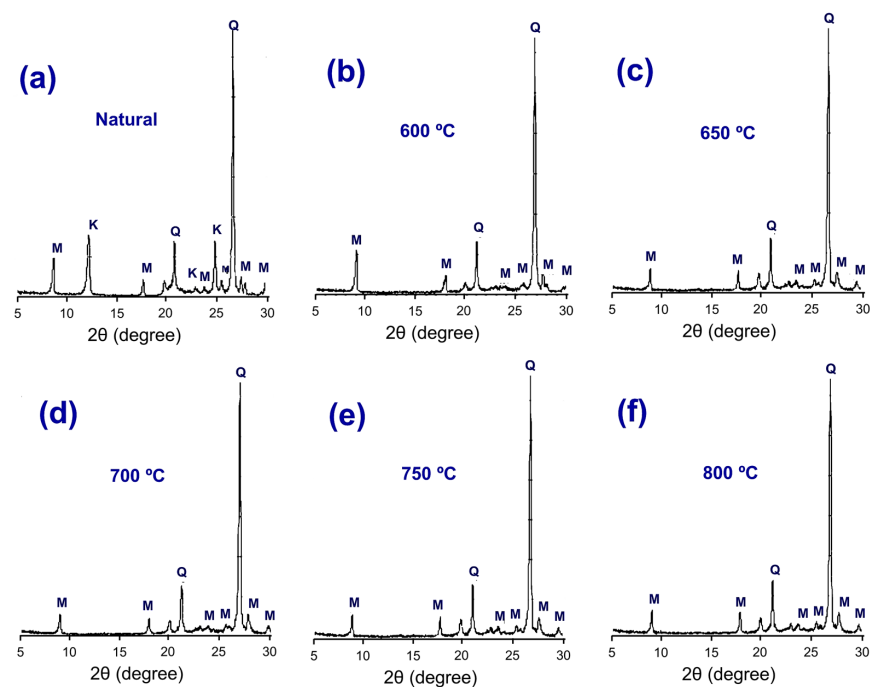


Figure 2. The XRD patterns measured from natural kaolin (a) and calcined residues at 600 °C (b), 650 °C (c), 700 °C (d), 750 °C (e), and 800 °C (f). (M: Mica, Q: Quartz, and K: Kaolinite).

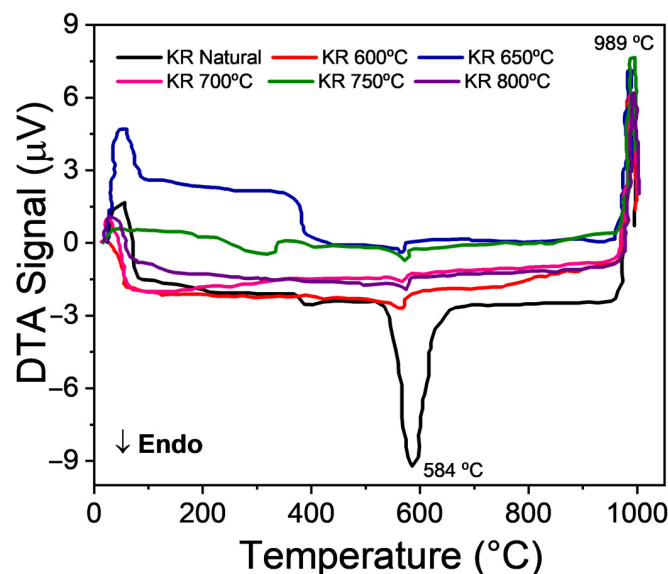


Figure 3. The DTA curves of natural and calcined kaolin residues at 600 °C, 650 °C, 700 °C, 750 °C, and 800 °C.

Table 3. The particle diameters of the Portland cement (PC), hydrated lime (HL), and natural and calcined kaolin residues (KR) at 600 °C, 650 °C, 700 °C, 750 °C, and 800 °C.

Diameter and Specific Area	Raw Materials							
	PC	HL	KR Natural	KR 600 °C	KR 650 °C	KR 700 °C	KR 750 °C	KR 800 °C
D ₁₀ (μm)	1.8	0.8	1.4	2.9	1.6	2.8	2.6	1.5
D ₅₀ (μm)	13.8	5.7	9.3	14.3	10.1	14.1	13.8	9.4
D ₉₀ (μm)	43.9	21.1	25.8	42.7	29.7	42.5	42.8	27.8
D _m (μm)	19.1	9.0	12.1	19.0	13.6	18.8	18.7	12.8
Specific area (m ² /g)	-	-	29.73	24.98	23.18	25.10	20.52	25.95

D₁₀ = Diameter at 10%; D₅₀ = Diameter at 50%; D₉₀ = Diameter at 90%; and D_m = Average diameter.

Figure 4 shows the compressive strength (CS) and the pozzolanic activity index (I_{PA}) measured from mortars without and with kaolin residue calcined at 800 °C (mortar ref. and mortar KR 800 °C, respectively). As previously mentioned, in the sample used to assess the I_{PA} value, 20% of the cement was replaced by calcined kaolin residue. All samples were cured for 7, 14, and 28 days. For samples cured for 7 days, it was observed that the addition of kaolin residue resulted in a decrease in compressive strength of 8.2% ($I_{PA} = 91.8\%$). Such behavior occurred because replacing part of the cement with pozzolan decreases its resistance, due to less cementing fraction. In addition, pozzolanic reactions are slow, so it is only with time that resistance increases. Such behavior is related to the formation of calcium silicate hydrate (CSH) resulting from the reaction between calcined kaolin residue and portlandite, i.e., a pozzolanic reaction. As expected, the CSH formation increases the mechanical strength. For cure times equal to 14 and 28 days, the mortar KR 800 °C sample showed slight CS values than the samples measured for the mortar ref. ($I_{PA} > 100\%$). From the perspective of mechanical strength, this result indicates that the kaolin residue, calcined at 800 °C, has the potential to replace cement in mortar. All I_{PA} values were higher than the minimum limit of 75% recommended by ASTM C618 [36].

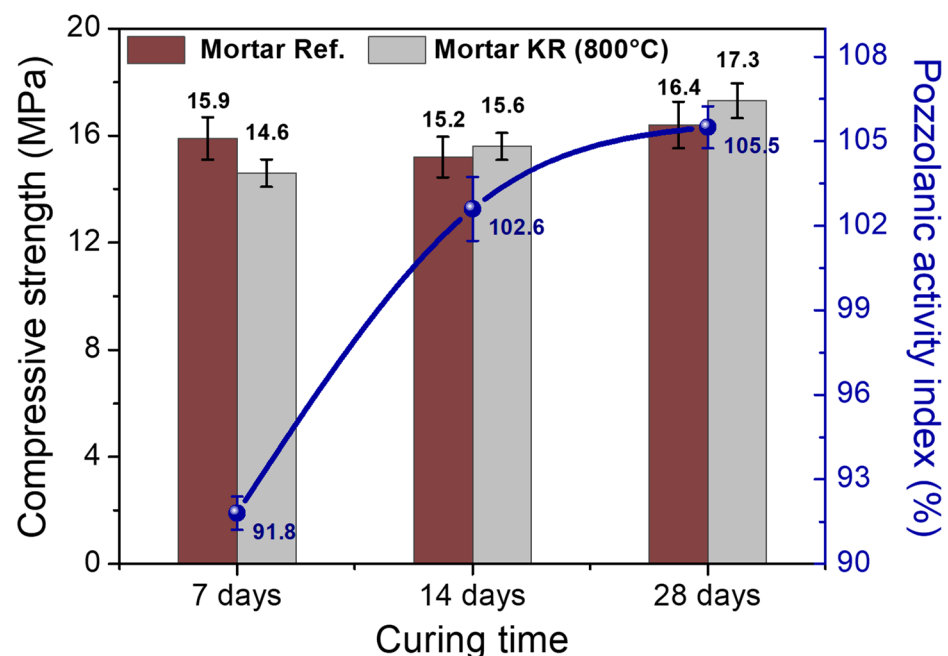


Figure 4. The compressive strength and pozzolanic activity index values for mortar ref. and mortar KR 800 °C samples.

3.2. Mortar Properties after Aging in Internal and External Environments

Figure 5a–e shows XRD patterns of mortar KR 800 °C aged under internal environments (E_i) for 30, 180, and 360 days (Figure 5a–c) and external environments (E_e) for

360 and 512 days (Figure 5d–e). The portlandite (Ca(OH)_2 , JCPDS 72-0156); ettringite ($3\text{CaO} \cdot \text{Al}_2\text{O}_3 \cdot 3\text{CaSO}_4 \cdot 32\text{H}_2\text{O}$, JCPDS 72-0646); calcite (CaCO_3 , JCPDS 05-0586); and quartz (SiO_2 , JCPDS 46-1045) were phases identified in the mortars exposed to the internal and external environment. However, the intensity of the portlandite phase peaks decreased with time. Such behavior is strongly related to the pozzolanic reactions and the carbonation process. This indicates that the pozzolanic reaction and the carbonation process, over time, have consumed the portlandite.

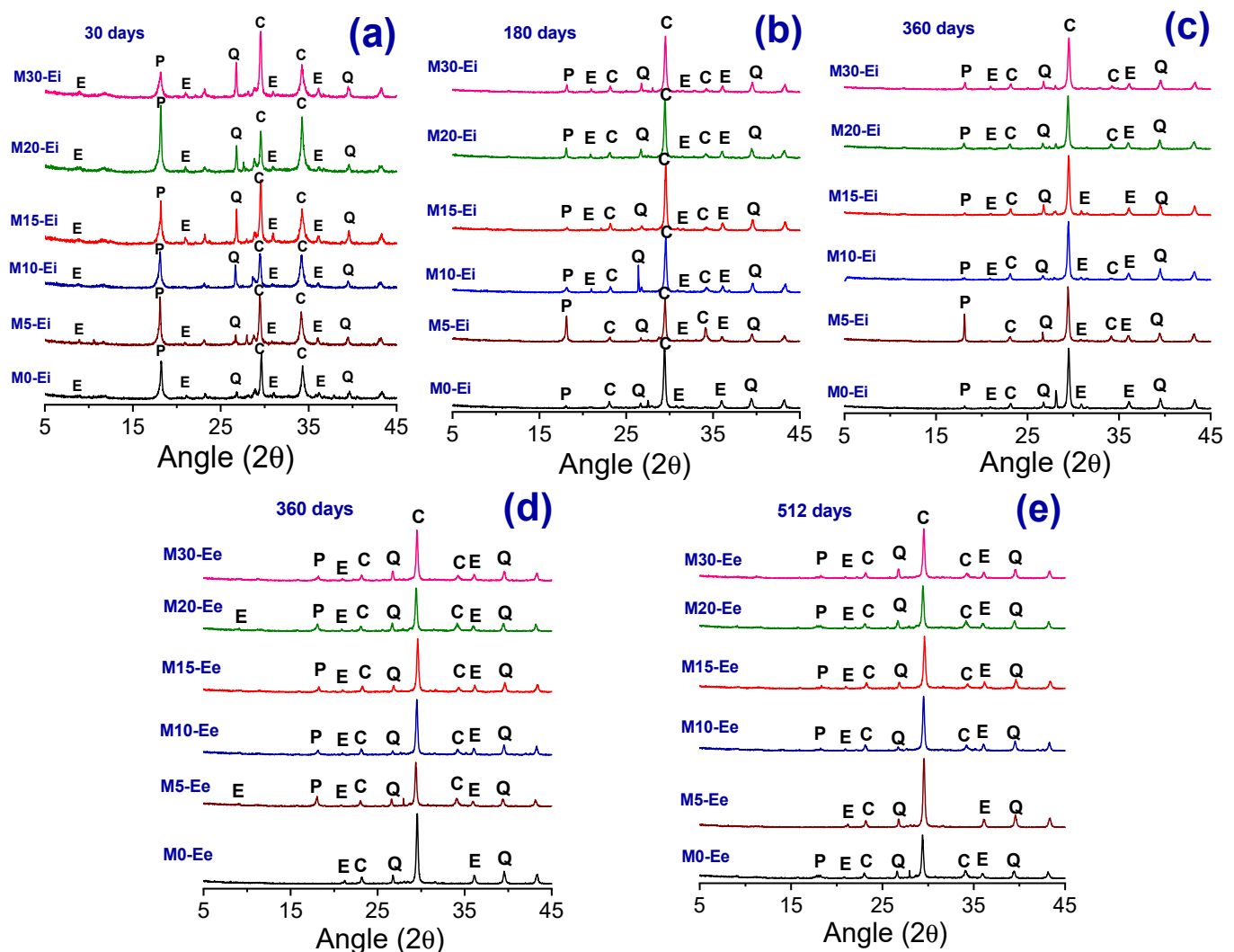


Figure 5. The XRD patterns of aged mortars in the internal environment of the laboratory for 30 days (a); 180 days (b); and 360 days (c), and of the exposure to the external environment for 360 days (d) and 512 days (e). (P: Portlandite, E: Ettringite, Q: Quartz, and C: Calcite).

Figure 6a–d show the TGA and DTA curves of mortars aged in an internal environment for 30 days (Figure 6a,b) and 360 days (Figure 6c,d). In general, it is possible to see that all the curves have a similar thermic profile. In summary, all mortars show four stages of mass loss. The first stage is identified in the temperature range between 25–100 °C and is associated with the evaporation of free water, adsorbed water loss, and water coordinated to cations. The second stage occurs in the temperature range between 101–400 °C and corresponds to the dehydration of ettringite, hydrated calcium silicate (CSH), and the decomposition of hemi compounds and monocarbonates (AFm). The dehydration regions of CSH and ettringite are superimposed; however, it is possible to observe peaks at around 156 °C which correspond to the loss of water in the ettringite phase [37–39].

The decomposition of hemi and monocarbonate components is more evident at 360 days (Figure 6d), a process in which it is possible to observe the formation of an endothermic band at around 215 °C. The last 2 stages occur in the temperature range between 401–500 °C and 501–1000 °C, and are related to the decomposition of calcium hydroxide ($\text{Ca}(\text{OH})_2 \rightarrow \text{CaO} + \text{H}_2\text{O}$) and calcium carbonate ($\text{CaCO}_3 \rightarrow \text{CaO} + \text{CO}_2$), respectively [40–42]. The mass loss in these regions can be used to determine the $\text{Ca}(\text{OH})_2$ and CaCO_3 content. It is worth mentioning that calcite (CaCO_3), a carbonation product, tends to reduce the mortars' strength.

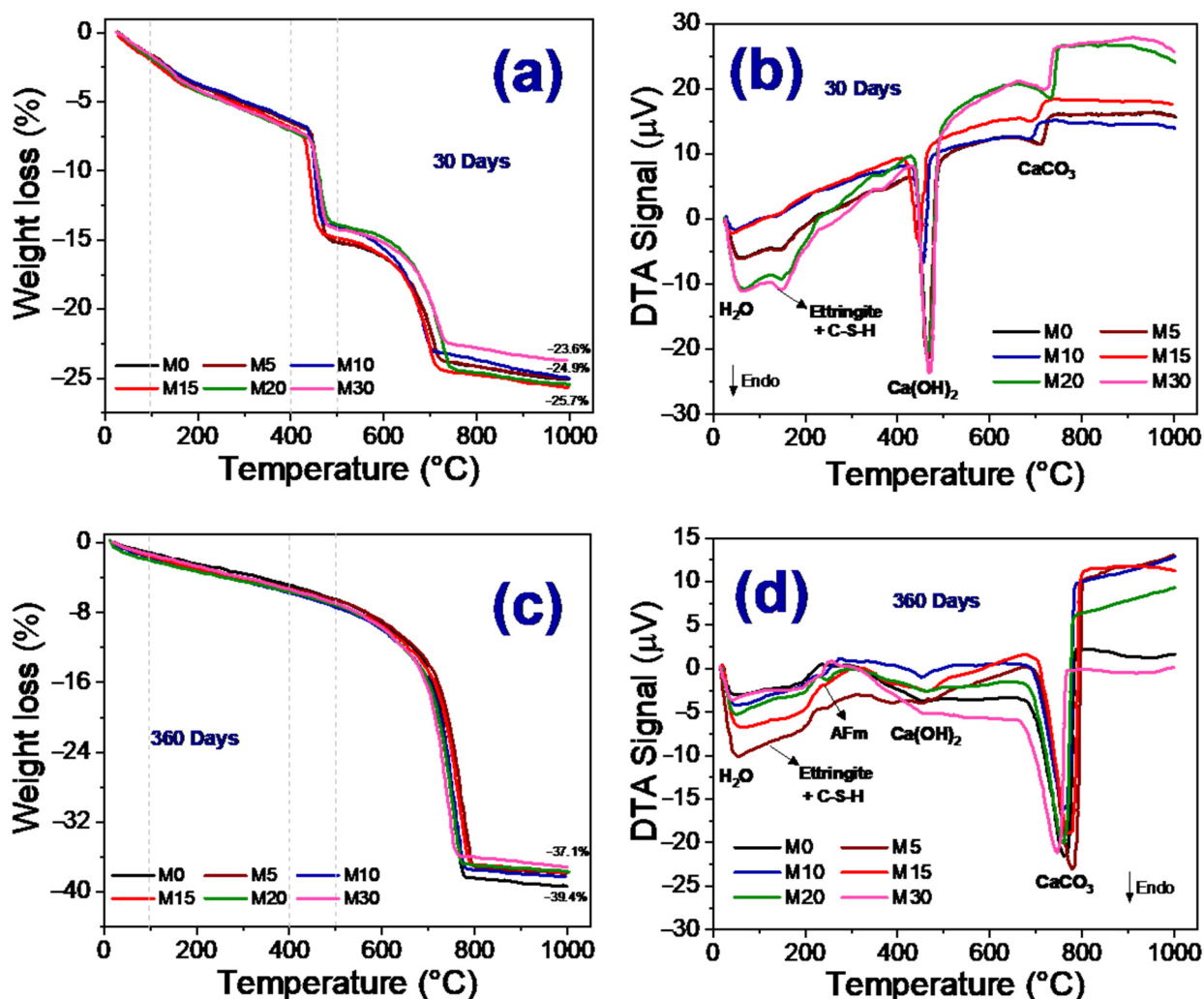


Figure 6. The TGA and DTA curves of mortars subjected to curing periods in an internal environment for 30 days (a,b) and 360 days (c,d). All the samples were heated with a heating rate of $12.5 \text{ }^\circ\text{C}/\text{min}^{-1}$ and up to $1000 \text{ }^\circ\text{C}$ in a nitrogen gas atmosphere.

An increase in loss was observed for all samples studied after 360 days of aging in the internal environment (Figure 6c,d). This result may be related to the exposure of the mortars to the ambient air, causing carbonation from the reaction with CO_2 . In fact, the intensity of the endothermic peaks related to calcite decomposition (CaCO_3) increases with time (see Figure 6b,d). Moreover, the intensity of the endothermic peaks, from the dehydroxylation of portlandite ($\text{Ca}(\text{OH})_2$) decreased significantly with time. This indicates that portlandite was consumed by the carbonation reaction.

For M0 (mortar without KR) the mass loss in the fourth region (i.e, the zone related to calcite decomposition) was approximately 18.6% and 32.7%, at 30 days and 360 days, respectively. However, for the samples with KR (M5, M10, M15, M20, and M30) the losses in this region were smaller, in the range of 9.9–11.6% and 30.4–31.6%, at 30 and 360 days.

This indicates that the formation of CSH was probably favored in the samples with calcined KR and, as a consequence, the carbonation effect was relatively moderate.

Figure 7a,b show the DTA curves of mortars aged naturally in an external environment for 90 days (Figure 7a) and 512 days (Figure 7b). For all compositions, endothermic peaks were observed at around 156 °C and 215 °C, which are related to ettringite and AFm (hemihydrate and monohydrate) phases, respectively [39,43]. It is known that calcined KR, in addition to silicon, has a high content of alumina in its composition (see Table 1). Thus, the presence of hemi and monohydrate compounds are probably associated with the chemical reaction of calcite (CaCO_3) from lime, and the extra alumina present in the system is likely due to the addition of kaolin residue. It is important to emphasize that the formation of hemi and monohydrate compounds inhibits the formation of monosulfate, so the ettringite remains in the system for a longer period of time [44]. The ettringite, hemi, and monohydrate phases occupy a greater volume of solid hydrates in the mortar pores compared to monosulfates, thus encouraging the filling up of voids and the attainment of mechanical strength [45].

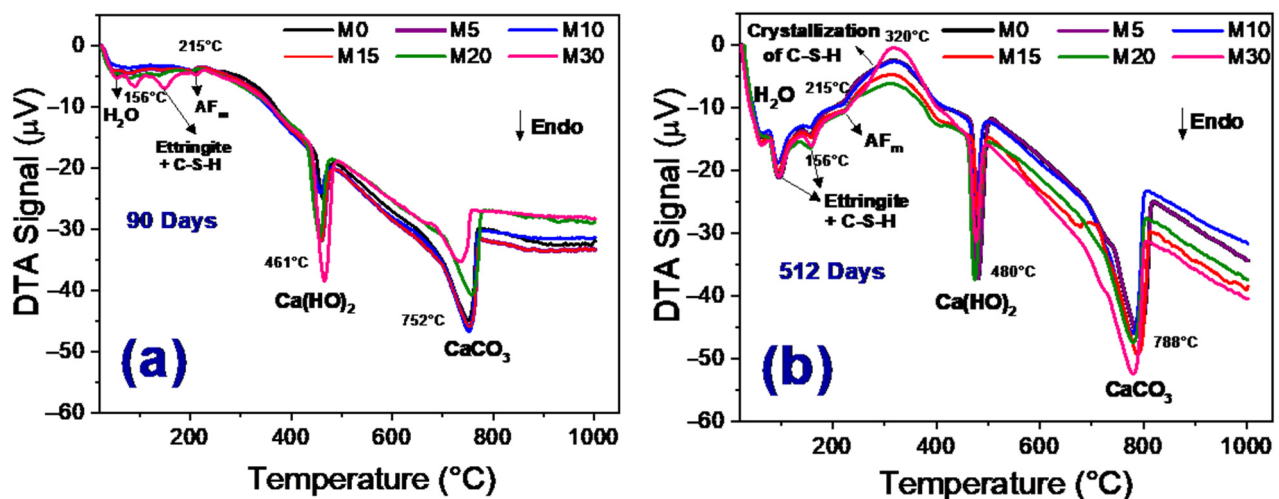


Figure 7. The DTA curves of mortars subjected to curing periods in an external environment for 90 days (a) and 512 days (b). All the samples were heated with a heating rate of $12.5\text{ }^{\circ}\text{C}/\text{min}^{-1}$ in a nitrogen gas atmosphere.

Intense peaks at $\sim 461\text{--}480\text{ }^{\circ}\text{C}$ and $\sim 750\text{ }^{\circ}\text{C}$ were also observed, which are associated with portlandite and calcium carbonate. This indicates that all mortars present an excess of free lime. The increase in the curing time from 90 to 512 days caused the displacement and intensification of the peak relative to calcium carbonate. With the displacement, the CaCO_3 peak occurred from $\sim 752\text{ }^{\circ}\text{C}$ to $\sim 788\text{ }^{\circ}\text{C}$. Such behavior is related to the consumption of portlandite by the pozzolanic reaction and carbonation.

In carbonation, CO_2 comes into contact with water and the carbonate elements ($\text{Ca}(\text{OH})_2$, C-S-H, C_2S , and C_3S) in the mortar pores. This process depends on relative humidity, temperature, and CO_2 concentration. Furthermore, the inefficient compaction and high water–cement ratio generate high permeability in the material [46]. For mortars cured at 512 days (Figure 7b), it is possible to observe the appearance of exothermic bands between the temperatures of 215–450 °C. These bands refer to the crystallization of CSH.

Figure 8a–f show the CS values and percentages of increase/decrease in the samples submitted to natural aging in the internal (Figure 8a,c,e) and external environments (Figure 8b,d,f). In Figure 8a, it is possible to observe an increase in the compressive strength of samples cured up to 180 days. Such behavior is related to the cement hydration process and the pozzolanic reactions.

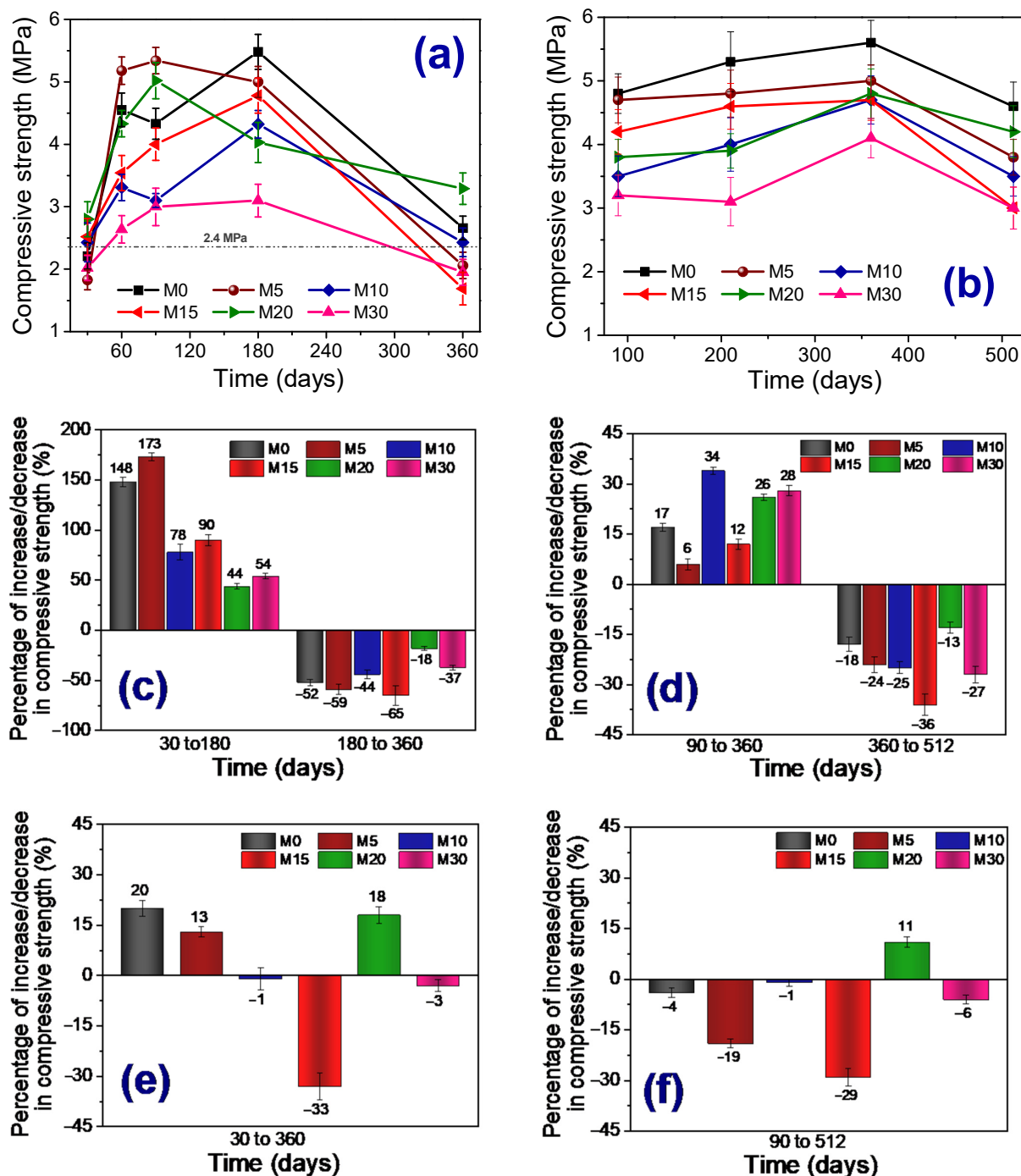


Figure 8. The compressive strength and the percentage of increase/decrease in the aged mortars in the internal environment of the laboratory for 30, 60, 90, 180, and 360 days (a,c,e), and the exposure to the external environment for 90; 210; 360; and 512 days (b,d,f).

The main products formed during the cement hydration process are hydrated calcium silicate (primarily CSH) and portlandite $\text{Ca}(\text{OH})_2$. CSH is a non-crystalline product, called agglomerating gel, that provides resistance to mortar and concrete and contributes significantly to the durability of cementitious materials. Moreover, due to the pore refinement process, there is a decrease in the permeability of the system and, therefore, a hinderance to the contact of reactive substances with the cement. On the other hand, portlandite consists of low resistance crystals that are soluble in water and which do not contribute to the material's resistance and durability [6,47,48].

In the pozzolanic reaction, the calcined kaolin residue (metakaolin) reacts with calcium hydroxide (portlandite) to form additional hydrated calcium silicate (secondary CSH), see Equation (2). Figure 9 shows the schematic representation of the microstructure of the material without pozzolan and with the incorporation of pozzolan. The CSH particles are smaller when compared to $\text{Ca}(\text{OH})_2$, and have the ability to occupy capillary voids. These particles also have a greater specific area, providing the cement paste with greater mechanical resistance [49].

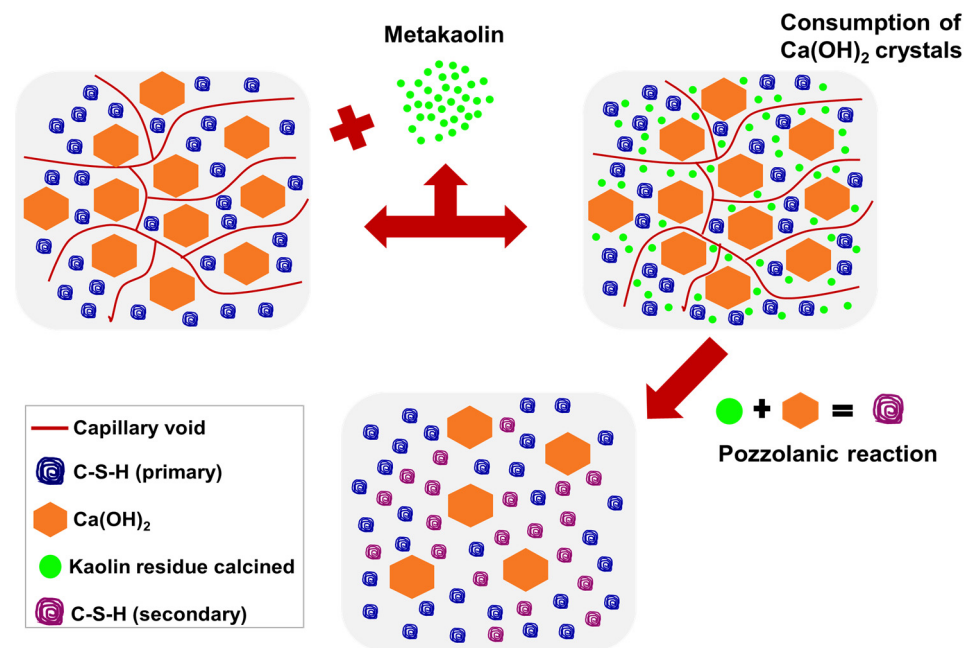
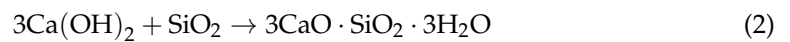
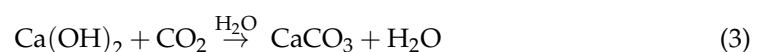


Figure 9. The schematic representation of the microstructure of cementitious material with and without the addition of pozzolan.

Regardless of the aging test type (internal and external environments), M10, M15, and M30 samples showed lower compressive strength values than the reference sample (M0). Moreover, at the end of the aging period in the internal environment (30 to 360 days), there was no resistance gain for M10, M15, and M30 samples. It is noteworthy that the M15 sample showed a 33% reduction in resistance to the initial cure time (30 days), see Figure 8e. These same mortars showed similar behavioral patterns when subjected to aging in an external environment (Figure 8d,f), which indicates that, although it has presented considerable initial gains, the replacement of cement with calcined kaolin residue, in the proportions of 10%, 15%, and 30%, did not lead to an improvement in its durability over time.

In general, there is a considerable decrease in the mechanical strength for all mortars with the evolution of the curing time ranging from 180 to 360 days (internal environment aging: Figure 8a) and from 360 to 512 days (external environment aging: Figure 8b). Such behavior can be associated with the carbonation process. Carbonation occurs due to carbon dioxide gas (CO_2), present in the air, penetrating the mortars through the pores in the material. In the presence of water, CO_2 dissolves and forms CO_3^{2-} ions which react with Ca^{2+} ions to form calcite, as shown in Equation (3). Ca^{2+} ions originate mainly from portlandite.



In addition to the portlandite, other hydrated compounds (calcium aluminates and silicates) are also sensitive to CO_2 attack. The reaction between CO_2 and $\text{Ca}(\text{OH})_2$ is more

favorable from a kinetics viewpoint. For example, the reaction between CO_2 and $\text{Ca}(\text{OH})_2$ is three times faster than the reaction between CO_2 and CSH , which is twenty times faster than the reaction between CO_2 and C_2S , and fifty times faster than the reaction between CO_2 and C_3S [17,50]. Figure 10 schematically shows the carbonation process that occurs when CO_2 enters the mortar surface through the pores in the material.

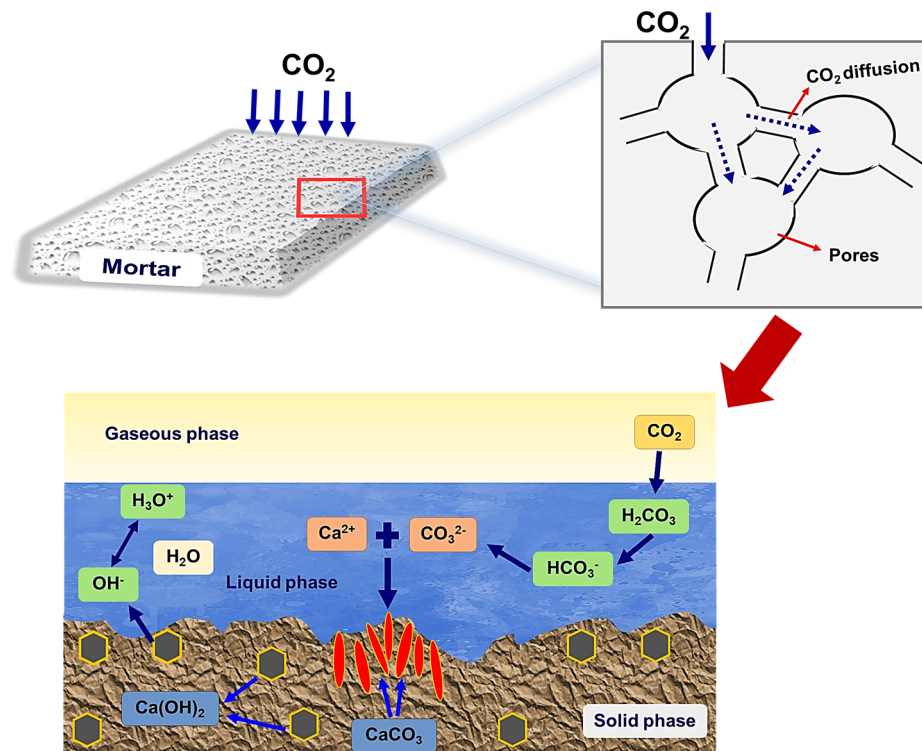


Figure 10. The schematic representation of the carbonation process.

The composition with 20% of residue (M20) presented the lowest percentage of resistance loss among all the compositions, and was the only case that, at the end of the whole process, presented resistance gain in both forms of aging (internal and external environments), see Figure 8e,f. At the end of the 360 days, in the internal environment aging test, the compressive strength of this composition surpassed the MPa of the other compositions (3.3 ± 0.25). This shows that, even with carbonation, the M20 sample degraded less. This behavior is probably associated with the greater packaging of particles, making CO_2 access more difficult and reducing the carbonation effect. Figure 11 shows the water absorption results (WA) of the mortars after the aging test in the internal environment. It is possible to observe that, at the end of the 360 days, M20 presented the lowest value of WA (12.6 ± 0.3)% compared with the other compositions. In this way, it is reasonable to infer that the M20 sample presented minor porosity, at least between 90 and 360 days of acting under the internal environment. Such a conclusion strengthens the idea of CO_2 access reducing the carbonation effect.

Therefore, the porosity present in the mortars and concretes is one factor that can affect durability and stability since it facilitates the aggressive agent diffusibility to the material, such as carbon dioxide, acidic solutions, and sulfides. Thus, it is essential to highlight the importance of studying the degradation behavior of mortars containing residues, since the result of their resistance, which is generally measured after curing in 28 days, does not always indicate the real behavior of this material over time. Furthermore, it is essential to consider the content of substitution for the use of residues in mortars. The M0, M10, and M20 samples presented resistance values within the minimum limit (2.4 MPa) established by ASTM C 270 [51] in both types of aging tests (internal and external environments).

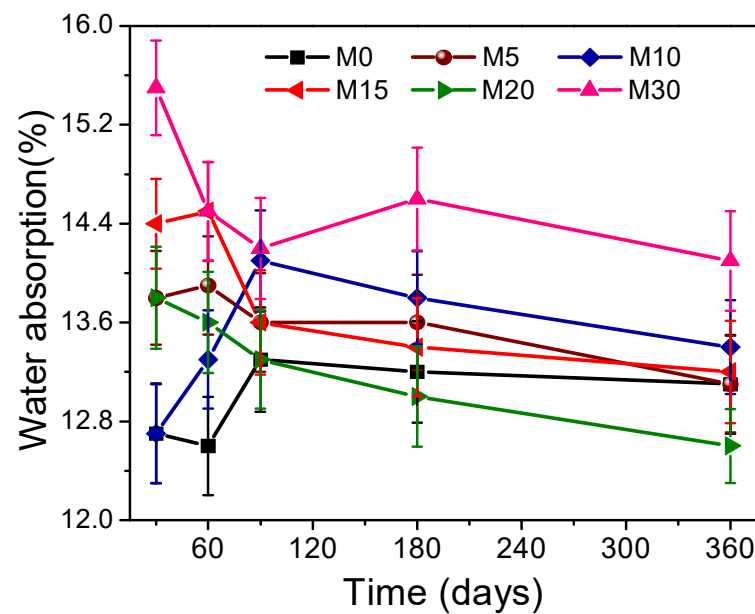


Figure 11. The water absorption of the aged mortars in the internal environment of the laboratory for 30, 60, 90, 180, and 360 days.

4. Conclusions

Based on our results, it can be concluded that the partial replacement of Portland cement with kaolin residue in coating mortars is feasible. The addition of calcined kaolin residue in the mortars reduced the mechanical resistance to compression in practically all substitution levels. However, mortars with a 10% and 20% substitution presented resistance values within the minimum limit of 2.4 MPa established by ASTM C 270. The content of replacing cement with a kaolin residue influenced the durability behavior of the mortars. Incorporating the residue in the substitution proportions of 5%, 10%, 15%, and 30% did not improve their mechanical resistance or durability. The composition with 20% of kaolin residues presented, again, compressive strength at the end of the entire aging process to the initial evaluation stages. And at the end of 360 days of aging in an internal environment, the compressive strength of this composition surpassed the MPa of the other compositions (3.3 ± 0.25).

Author Contributions: Methodology, software, data curation, and formal analysis, F.P.d.C., S.L.D.B. and J.V.F.; conceptualization, supervision, funding acquisition, and project administration, G.d.A.N. and R.R.M.; formal analysis and writing—review and editing, A.M.R. All authors have read and agreed to the published version of the manuscript.

Funding: This research was funded by Coordenação de Aperfeiçoamento de Pessoal de Nível Superior (CAPES), grant number 88887.597478/2021-00, and by Conselho Nacional de Desenvolvimento Científico e Tecnológico (CNPq), grant number 140211/2021-7.

Data Availability Statement: Not applicable.

Acknowledgments: The authors would like to thank the Laboratório de Tecnologia do Materiais (LTM-UAEMa/UFCEG) for the infrastructure to carry out tests.

Conflicts of Interest: The authors declare no conflict of interest.

References

1. Amaral, L.F.; Girondi Delaqua, G.C.; Nicolite, M.; Marvila, M.T.; de Azevedo, A.R.G.; Alexandre, J.; Fontes Vieira, C.M.; Monteiro, S.N. Eco-friendly mortars with addition of ornamental stone waste—A mathematical model approach for granulometric optimization. *J. Clean. Prod.* **2020**, *248*, 119283. [[CrossRef](#)]
2. Cree, D.; Pliya, P. Effect of elevated temperature on eggshell, eggshell powder and eggshell powder mortars for masonry applications. *J. Build. Eng.* **2019**, *26*, 100852. [[CrossRef](#)]

3. McLellan, B.C.; Williams, R.P.; Lay, J.; Van Riessen, A.; Corder, G.D. Costs and carbon emissions for geopolymer pastes in comparison to ordinary portland cement. *J. Clean. Prod.* **2011**, *19*, 1080–1090. [[CrossRef](#)]
4. Chen, Z.; Poon, C.S. Comparative studies on the effects of sewage sludge ash and fly ash on cement hydration and properties of cement mortars. *Constr. Build. Mater.* **2017**, *154*, 791–803. [[CrossRef](#)]
5. Bilir, T.; Gencel, O.; Topcu, I. Properties of mortars with fly ash as fine aggregate. *Constr. Build. Mater.* **2015**, *93*, 782–789. [[CrossRef](#)]
6. Hsu, S.; Chi, M.; Huang, R. Effect of fineness and replacement ratio of ground fly ash on properties of blended cement mortar. *Constr. Build. Mater.* **2018**, *176*, 250–258. [[CrossRef](#)]
7. Onn, C.C.; Mo, K.H.; Radwan, M.K.; Liew, W.H.; Ng, C.G.; Yusoff, S. Strength, carbon footprint and cost considerations of mortar blends with high volume ground granulated blast furnace slag. *Sustainability* **2019**, *11*, 7194. [[CrossRef](#)]
8. Seifi, S.; Sebaibi, N.; Levacher, D.; Boutouil, M. Mechanical performance of a dry mortar without cement, based on paper fly ash and blast furnace slag. *J. Build. Eng.* **2019**, *22*, 113–121. [[CrossRef](#)]
9. Rakhimova, N.; Rakhimov, R.Z. Alkali-activated cements and mortars based on blast furnace slag and red clay brick waste. *Mater. Des.* **2015**, *85*, 324–331. [[CrossRef](#)]
10. Pliya, P.; Cree, D. Limestone derived eggshell powder as a replacement in Portland cement mortar. *Constr. Build. Mater.* **2015**, *95*, 1–9. [[CrossRef](#)]
11. Ahmad, M.; Chen, B. Effect of silica fume and basalt fiber on the mechanical properties and microstructure of magnesium phosphate cement (MPC) mortar. *Constr. Build. Mater.* **2018**, *190*, 466–478. [[CrossRef](#)]
12. Benli, A. Mechanical and durability properties of self-compacting mortars containing binary and ternary mixes of fly ash and silica fume. *Struct. Concr.* **2019**, *20*, 1096–1108. [[CrossRef](#)]
13. Gupta, S.; Kua, H.W. Combination of Biochar and Silica Fume as Partial Cement Replacement in Mortar: Performance Evaluation Under Normal and Elevated Temperature. *Waste Biomass Valorization* **2020**, *11*, 2807–2824. [[CrossRef](#)]
14. Chouhan, H.S.; Kalla, P.; Nagar, R.; Gautam, P.K. Gainful utilization of dimensional limestone waste as fine aggregate in cement mortar mixes. *Constr. Build. Mater.* **2019**, *221*, 363–374. [[CrossRef](#)]
15. Pozo-Antonio, J. Evolution of mechanical properties and drying shrinkage in lime-based and lime cement-based mortars with pure limestone aggregate. *Constr. Build. Mater.* **2015**, *77*, 472–478. [[CrossRef](#)]
16. Hanjitsuwan, S.; Phoo-ngernkham, T.; Li, L.Y.; Damrongwiriyapunap, N.; Chindapasirt, P. Strength development and durability of alkali-activated fly ash mortar with calcium carbide residue as additive. *Constr. Build. Mater.* **2018**, *162*, 714–723. [[CrossRef](#)]
17. Sabir, B.; Wild, S.; Bai, J. Metakaolin and calcined clays as pozzolans for concrete: A review. *Cem. Concr. Compos.* **2001**, *23*, 441–454. [[CrossRef](#)]
18. Koutník, P.; Soukup, A.; Bezucha, P.; Šafař, J.; Kohout, J. Low viscosity metakaolinite based geopolymer binders. *Constr. Build. Mater.* **2020**, *230*, 116978. [[CrossRef](#)]
19. Silva, A.S.; Gameiro, A.; Grilo, J.; Veiga, R.; Velosa, A. Long-term behavior of lime-metakaolin pastes at ambient temperature and humid curing condition. *Appl. Clay Sci.* **2014**, *88–89*, 49–55. [[CrossRef](#)]
20. Al-Akhras, N.M. Durability of metakaolin concrete to sulfate attack. *Cem. Concr. Res.* **2006**, *36*, 1727–1734. [[CrossRef](#)]
21. Güneysi, E.; Gesoğlu, M.; Mermerdaş, K. Improving strength, drying shrinkage, and pore structure of concrete using metakaolin. *Mater. Struct.* **2008**, *41*, 937–949. [[CrossRef](#)]
22. Bassuoni, M.T.; Nehdi, M.L. Resistance of self-consolidating concrete to sulfuric acid attack with consecutive pH reduction. *Cem. Concr. Res.* **2007**, *37*, 1070–1084. [[CrossRef](#)]
23. Goyal, S.; Kumar, M.; Sidhu, D.S.; Bhattacharjee, B. Resistance of Mineral Admixture Concrete to Acid Attack. *J. Adv. Concr. Technol.* **2009**, *7*, 273–283. [[CrossRef](#)]
24. Senhadji, Y.; Escadeillas, G.; Khelafi, H.; Mouli, M.; Benosman, A.S. Evaluation of natural pozzolan for use as supplementary cementitious material. *Eur. J. Environ. Civ. Eng.* **2012**, *16*, 77–96. [[CrossRef](#)]
25. ASTM International. *ASTM C150/C150M-20, Standard Specification for Portland Cement*; ASTM International: West Conshohocken, PA, USA, 2020.
26. ASTM International. *ASTM C1437, Standard Test Method for Flow of Hydraulic Cement Mortar*; ASTM International: West Conshohocken, PA, USA, 2020.
27. ASTM International. *ASTM C311-18-Standard Test Methods for Sampling and Testing Fly Ash or Natural Pozzolans for Use in Portland-Cement Concrete*; ASTM International: West Conshohocken, PA, USA, 2018.
28. ASTM International. *ASTM C39/C39M-20-Standard Test Method for Compressive Strength of Cylindrical Concrete Specimens*; ASTM International: West Conshohocken, PA, USA, 2020.
29. Huang, Y.; Deng, J.; Wang, W.; Feng, Q.; Xu, Z. Preliminary investigation of pozzolanic properties of calcined waste kaolin. *Medziagotyra* **2018**, *24*, 177–184. [[CrossRef](#)]
30. Almeida, E.P.; Carreiro, M.E.A.; Rodrigues, A.M.; Ferreira, H.S.; Santana, L.N.L.; Menezes, R.R.; Neves, G.A. A new eco-friendly mass formulation based on industrial mining residues for the manufacture of ceramic tiles. *Ceram. Int.* **2020**. [[CrossRef](#)]
31. Da Silva, V.J.; da Silva, M.F.; Gonçalves, W.P.; de Menezes, R.R.; de Araújo Neves, G.; de Lucena Lira, H.; de Lima Santana, L.N. Porous mullite blocks with compositions containing kaolin and alumina waste. *Ceram. Int.* **2016**, *42*, 15471–15478. [[CrossRef](#)]
32. Bui, D.D.; Hu, J.; Stroeven, P. Particle size effect on the strength of rice husk ash blended gap-graded Portland cement concrete. *Cem. Concr. Compos.* **2005**, *27*, 357–366. [[CrossRef](#)]

33. Kiattikomol, K.; Jaturapitakkul, C.; Songpiriyakij, S.; Chutubtim, S. A study of ground coarse fly ashes with different finenesses from various sources as pozzolanic materials. *Cem. Concr. Compos.* **2001**, *23*, 335–343. [[CrossRef](#)]
34. Da Costa, F.P.; da Silva Morais, C.R.; Rodrigues, A.M. Sustainable glass-ceramic foams manufactured from waste glass bottles and bentonite. *Ceram. Int.* **2020**, *46*, 17957–17961. [[CrossRef](#)]
35. Da Costa, F.P.; da Silva Morais, C.R.; Pinto, H.C.; Rodrigues, A.M. Microstructure and physico-mechanical properties of Al₂O₃-doped sustainable glass-ceramic foams. *Mater. Chem. Phys.* **2020**, *256*, 123612. [[CrossRef](#)]
36. ASTM International. *ASTM C618-19-Standard Specification for Coal Fly Ash and Raw or Calcined Natural Pozzolan for Use in Concrete 1*; ASTM International: West Conshohocken, PA, USA, 2019. [[CrossRef](#)]
37. Sun, C.; Sun, M.; Tao, T.; Qu, F.; Wang, G.; Zhang, P.; Li, Y.; Duan, J. Chloride binding capacity and its effect on the microstructure of mortar made with marine sand. *Sustainability* **2021**, *13*, 4169. [[CrossRef](#)]
38. Michel, M.; Georjgin, J.F.; Ambroise, J. Improving the mechanical performance of high-grade slag cement by the addition of Portland cement and sulfoaluminate cement. *Constr. Build. Mater.* **2012**, *37*, 291–300. [[CrossRef](#)]
39. De Weerd, K.; Kjellsen, K.O.; Sellevold, E.; Justnes, H. Synergy between fly ash and limestone powder in ternary cements. *Cem. Concr. Compos.* **2011**, *33*, 30–38. [[CrossRef](#)]
40. Song, H.; Jeong, Y.; Bae, S.; Jun, Y.; Yoon, S.; Oh, J.E. A study of thermal decomposition of phases in cementitious systems using HT-XRD and TG. *Constr. Build. Mater.* **2018**, *169*, 648–661. [[CrossRef](#)]
41. Liu, C.; Yang, L.; Wang, F.; Hu, S. Enhance the durability of heat-cured mortars by internal curing and pozzolanic activity of lightweight fine aggregates. *Constr. Build. Mater.* **2021**, *270*, 121439. [[CrossRef](#)]
42. Rupasinghe, M.; Nicolas, R.S.; Mendis, P.; Sofi, M.; Ngo, T. Investigation of strength and hydration characteristics in nano-silica incorporated cement paste. *Cem. Concr. Compos.* **2017**, *80*, 17–30. [[CrossRef](#)]
43. Krishnan, S.; Bishnoi, S. Understanding the hydration of dolomite in cementitious systems with reactive aluminosilicates such as calcined clay. *Cem. Concr. Res.* **2018**, *108*, 116–128. [[CrossRef](#)]
44. Antoni, M.; Rossen, J.; Martirena, F.; Scrivener, K. Cement substitution by a combination of metakaolin and limestone. *Cem. Concr. Res.* **2012**, *42*, 1579–1589. [[CrossRef](#)]
45. Zajac, M.; Rossberg, A.; Le Saout, G.; Lothenbach, B. Influence of limestone and anhydrite on the hydration of Portland cements. *Cem. Concr. Compos.* **2014**, *46*, 99–108. [[CrossRef](#)]
46. Nasser, A.; Clément, A.; Laurens, S.; Castel, A. Influence of steel–concrete interface condition on galvanic corrosion currents in carbonated concrete. *Corros. Sci.* **2010**, *52*, 2878–2890. [[CrossRef](#)]
47. Heukamp, F.H.; Ulm, F.-J.; Germaine, J.T. Poroplastic properties of calcium-leached cement-based materials. *Cem. Concr. Res.* **2003**, *33*, 1155–1173. [[CrossRef](#)]
48. Singh, M.; Garg, M. Reactive pozzolana from Indian clays—their use in cement mortars. *Cem. Concr. Res.* **2006**, *36*, 1903–1907. [[CrossRef](#)]
49. Morandeau, A.; Thiery, M.; Dangla, P. Investigation of the carbonation mechanism of CH and CSH in terms of kinetics, microstructure changes and moisture properties. *Cem. Concr. Res.* **2014**, *56*, 153–170. [[CrossRef](#)]
50. Aguirre-Guerrero, A.M.; Mejía-de-Gutiérrez, R.; Montês-Correia, M.J.R. Corrosion performance of blended concretes exposed to different aggressive environments. *Constr. Build. Mater.* **2016**, *121*, 704–716. [[CrossRef](#)]
51. ASTM International. *ASTM C270-19-Standard Specification for Mortar for Unit Masonry*; ASTM International: West Conshohocken, PA, USA, 2019.